www.icgst.com

Extension of the Sub-pixel Efficacy Region to the Lagrange Interpolation Function

Carlo Ciulla and Fadi P. Deek [1*]

[1] *College of Science and Liberal Arts, New Jersey Institute of Technology*
323 M.L.King Blvd. University Heights - Newark, NJ 07102-1982, USA
[*] Corresponding author; [cxc2728, Fadi.Deek]@NJIT.EDU

Abstract

This paper reports on a novel methodology for improving the approximation properties of the cubic form of the Lagrange interpolation function through the use of two mathematical formulations: (i) the Intensity-Curvature Functional (ΔE) and (ii) its derived Sub-pixel Efficacy Region (SRE). Equations are determined dependent on the local curvature of the interpolation function and the pixel intensity at the neighbourhood, thus making it possible to calculate the Lagrange function with improved approximation properties. Characterizations of interpolation error and interpolation error improvement bounds are also presented. Fast Fourier Transform and Root-mean-square-error analyses are used to realize and present the improvements. The significance of the results is discussed within the context of a unifying framework which uses the same methodology for the improvement of the interpolation error of diverse functions.

Keywords: *Lagrange Interpolation, Intensity-Curvature Functional, Sub-pixel Efficacy Region.*

1. Introduction

1.1 Background

In general, reports from the literature describe Lagrange approximation error bounds that are dependent on the sampling step [1, 2] and also on the Hilbert Transform [3]. Error bounds based on the sampling step were also obtained within the context of approximation theory [4], and based on which, various other interpolation schemes have also been recently developed [5-7]. According to such results, given a continuous function, h: R → R that is derivable up till the n^{-th} order, a kernel β: R → R, and a set of coefficients α_k that incorporates the value of h at the neighbourhood, the h function can be represented by the convolution:

$$h_\ell(x) = \Sigma_k \alpha_k \beta [(x / \ell) - k] \quad (1)$$

where ℓ is the sampling step. It is true that: $\| h - h_\ell \|_L^2 \leq \varepsilon \ell^n \| h^{(n)} \|_L^2$; where L^2 is the L^2-norm, ε is a given constant, and $h^{(n)}$ the n^{-th} order derivative of the h function [4]. Thus, the interpolation error is bounded by the sampling step. For the given definition of $h_\ell(x)$, the above concept can then be intuitively understood considering the increasing degree of uncertainty of estimation for the increasing size of ℓ, because of the increasing lack of certainty of the true local curvature of the unknown signal for $x \in [-\ell,\ell]$. Therefore, it is logical to presuppose that with increasing ℓ, there is an increase in interpolation error.

The literature is indeed lacking a theoretical approach that is capable to: (i) quantify the effect of the interpolator on the signal in terms of the joint information content of node intensity and second order derivative of the interpolation function, and based on this, (ii) to determine interpolation error improvement. The development of a mathematical formulation with above characteristics and the derivation, by deduction, of a unifying framework for the improvement of the interpolation error has been done for other interpolation paradigms, including the bivariate linear [8], trivariate linear and B-Splines [9]. Intuitions constituted by the Intensity-Curvature Functional (ΔE) and the Sub-Pixel Efficacy Region (SRE), the former being a mathematical formulation embedding the effect of the interpolation function on the pixel intensity and the latter being a space domain set of points obtained from the study of ΔE, allowed the conceptualization of novel forms interpolators called SRE-based interpolation functions [8, 9]. They have improved approximation characteristics, and they are capable of performing re-sampling at locations that vary pixel-by-pixel. Using the concept of curvature of the interpolation function, these intuitions, as well as the novel theory derived from them, bridge the gap with the theoretical basis of classic interpolation.

1.2 Motivations of the Present Work

The motivation for this work is of two-fold: First, the theory presented in [8, 9] and applied to bivariate,

trivariate liner, quadratic B-Spline interpolation functions, motivates the effort of setting the grounds for the establishment of a unifying framework for the improvement of the interpolation error. Second, we show that both the theory and the unifying framework emanating from it have applicability also to the cubic Lagrange interpolation function. This fact is of relevance to the extent that for a theory to be comprehensive, it needs to cover the most possible cases based on the least number of mathematical axioms and formulations, which are in this case: (i) the Intensity-Curvature Functional (ΔE), and (ii) the Sub-Pixel Efficacy Region (SRE). Therefore, this paper, while giving an overview of the capability of the unifying framework in improving the interpolation error, extends the theory to the Lagrange function, and for the latter formulates ΔE and derives the SRE. In addition, it is given a demonstration that the mathematical formulation proposed here furnishes the basis for the interpolation error and its improvement to be bounded by two constants.

The remaining parts of the paper are organized as follows: section two outlines the theory relevant to the Lagrange function together with the presentation of the two theorems; section three presents an overview of the results; and section four presents a discussion of these results, placing emphasis on the benefits and limitations of the theory advanced by this work.

2. Theory

2.1 Aim

The basic aim of this work is to develop a mathematical formulation that yields improvement in the Lagrange interpolation error. This is achieved through two mathematical methods that bridge classic interpolation with the theory presented here. They are: (i) the Intensity-Curvature Functional (ΔE), which is dependent on the local properties of the discrete signal and the curvature of the function, and (ii) the Sub-pixel Efficacy Region (SRE) defined next. The approach states the formulation of ΔE, analyzes it, and derives the SRE, by which the interpolator assumes improved approximation characteristics.

2.2 The Interpolation Function

The one dimensional Lagrange interpolation function that was studied is reported in [10] as:

$$LGR_3(x) = \begin{cases} (1/2)\,|x|^3 - |x|^2 - (1/2)\,|x| + 1 & 0 \le |x| \le 1 \\ -(1/6)\,|x|^3 + |x|^2 - (11/6)\,|x| + 1 & 1 \le |x| \le 2 \end{cases} \quad (2)$$

It is considered here with a 2 x 2 neighbourhood f(-1), f(1), f(-2), f(2) centred at f (0).

2.3 The Intensity-Curvature Functional

ΔE = ΔE(x) is defined as the ratio between the Intensity-Curvature term calculated at the grid point (x = 0) and named E_o, and at the generic intra-node location (x ≠ 0) and named E_{IN}. Let those be defined as:

$\theta = (\partial^2 (LGR_3(x))/\partial x^2)_{x=0} = (-2\,\theta^{(1)} + 2\,\theta^{(2)})$
$\theta^{(1)} = \pm [\, f(-1) + f(1) \,]$
$\theta^{(2)} = \pm [f(-2) + f(-1) + f(1) + f(2)]$
$\theta_1 = (-2\,\theta^{(1)} + 2\,\theta^{(2)}\theta^{(2)}) + 2\,f(0)\,[\theta^{(2)} - \theta^{(1)}]$
$\theta_2 = \{[2\,\theta^{(1)} + (7/3)\,\theta^{(1)}\theta^{(2)} - (7/3)\,\theta^{(2)}\theta^{(2)} + f(0)\,[(3/2)\,\theta^{(1)} - (1/2)\,\theta^{(2)}]\}$
$\theta_3 = [(1/6)\,\theta^{(1)} - (21/6)\,\theta^{(1)}\theta^{(2)} - (23/18)\,\theta^{(2)}\theta^{(2)}]$
$\theta_4 = [-(33/4)\,\theta^{(1)} + (27/12)\,\theta^{(1)}\theta^{(2)} - (7/12)\,\theta^{(2)}\theta^{(2)}]$
$\theta_5 = [-(3/20)\,\theta^{(1)} - (11/120)\,\theta^{(1)}\theta^{(2)}]$
$\theta_6 = [(3/2)\,\theta^{(1)}\theta^{(1)} - \theta^{(1)}\theta^{(2)} + (1/6)\,\theta^{(2)}\theta^{(2)}]$
$\theta_7 = [-\theta^{(1)} - 3\,\theta^{(1)}\theta^{(1)} + (16/3)\,\theta^{(1)}\theta^{(2)} - (4/3)\,\theta^{(2)}\theta^{(2)}]$
$\theta_8 = [(1/2)\,\theta^{(1)}\theta^{(1)} - (15/2)\,\theta^{(1)}\theta^{(2)} + (23/6)\,\theta^{(2)}\theta^{(2)}]$
$\theta_9 = [\, f(0)\,(3\,\theta^{(1)} - \theta^{(2)}) + 4\,\theta^{(1)}\theta^{(1)} + (14/3)\,\theta^{(1)}\theta^{(2)} - (14/3)\,\theta^{(2)}\theta^{(2)}]$
$\theta_{10} = [f(0)\,(2\,\theta^{(2)} - 2\,\theta^{(1)}) - 2\,\theta^{(1)}\theta^{(1)} + 2\,\theta^{(2)}\theta^{(2)}]$

Table 1: Values of theta for Eqs. (5), (6) and (13).

$$E_o = E_o(x) = \int_0^x f(0)\,(\partial^2 (LGR_3(x))/\partial x^2)_{x=0}\,dx \quad (3)$$

$$E_{IN} = E_{IN}(x) = \int_0^x LGR_3(x)\,\partial^2 (LGR_3(x))/\partial x^2\,dx \quad (4)$$

And they are calculated as:

$$E_o(x) = \int_0^x f(0)\,\theta\,dx = f(0)\,\theta\,x \quad (5)$$

$$E_{IN}(x) = \int_0^x \{f(0) + \theta^{(1)}\,[(1/2)\,|x|^3 - |x|^2 - (1/2)\,|x| + 1] + \theta^{(2)}\,[-(1/6)\,|x|^3 + |x|^2 - (11/6)\,|x| + 1]\} * \{\theta^{(1)}\,(3\,|x| - 2) + \theta^{(2)}\,(-|x| + 2)\}\,dx = x^5\theta_5 + x^4\theta_4 + x^3\theta_3 + x^2\theta_2 + x\theta_1 \quad (6)$$

All theta values of above positions, as reported in Table 1, make the expression of $E_o(x)$ and $E_{IN}(x)$ dependent on the relationships between the pixel intensity f(0) and its

neighbourhood of values, and so for the Intensity-Curvature Functional $\Delta E(x) = E_o(x) / E_{IN}(x)$, and as it can be seen next, also for the novel re-sampling locations $(x^{r(1,i)}, x^{r(2,i)}, x^{r(3,i)}, x^{r(4,i)})$ for i = 1, 2…4, where the Lagrange interpolation function is calculated.

2.4 Study of the Intensity-Curvature Functional

By equating the first order derivative of ΔE to zero, we obtain:

$$\partial(\Delta E(x))/\partial x = (E_o(x) * \partial(E_{IN}(x))/\partial x + E_{IN}(x) * \partial(E_o(x))/\partial x) / (E_{IN}(x))^2 = 0 \quad (7)$$

The above position furnishes the Sub-pixel Efficacy Region (SRE) of the Lagrange interpolation function (2) as:

$$6 x^4 \theta_5 + 5 x^3 \theta_4 + 4 x^2 \theta_3 + 3 x \theta_2 + 2 \theta_1 = 0 \quad (8)$$

For which the solution is given by the sub-pixel space points $x = x_{sre} \in \{x_{sre}^{(i)}, i = 1, 2…4\}$ that are reported in Table 2.

$x_{sre}^{(4)} = (-\alpha \pm \sqrt{\alpha^2 - \beta}) / 2$
$x_{sre}^{(3)} = (\theta_1 / 3\theta_5) / x_{sre}^{(4)}$
$x_{sre}^{(2)} = \{-\gamma \pm [\gamma^2 - (\beta / x_{sre}^{(4)} x_{sre}^{(3)})]^{1/2}\} / 2$
$x_{sre}^{(1)} = [-(5\theta_4 / 6\theta_5) - x_{sre}^{(4)} - x_{sre}^{(3)} - x_{sre}^{(2)}]$
$\alpha = [(\theta_2 / 2\theta_5) - (5\theta_1\theta_4 / 18\theta_5^2)] / [1 - (\theta_1 / 3\theta_5)]$
$\beta = (4\theta_1 / 3\theta_5)$
$\gamma = [(5\theta_4 / 6\theta_5) + x_{sre}^{(4)} + x_{sre}^{(3)}]$

Table 2. SRE sub-pixel space points.

In the remainder of the text the notation: $(\partial^2 (LGR_3(x))/\partial x^2)(x_{sre} - x^{r0})$ is the second order derivative of $LGR_3(x)$, with respect to the variable x, calculated at the location $(x_{sre} - x^{r0})$. Also, $(\partial^2 (LGR_3(x))/\partial x^2)(x_{sre})$ is the second order derivative of $LGR_3(x)$, with respect to the variable x, calculated at the location (x_{sre}).

2.5 Determination of the Novel Re-Sampling Locations

The SRE sub-pixel space points furnish the novel re-sampling locations where the Lagrange interpolation has improved approximation properties. Given a misplacement x_0, any novel re-sampling location $x^{r0} \in \{x^{r(1,i)}, x^{r(2,i)}, x^{r(3,i)}, x^{r(4,i)}, i = 1, 2…4\}$ is found by the process starting for each $x_{sre} \in \{x_{sre}^{(i)}, i = 1, 2…4\}$, from the equation:

$$\{LGR_3(x_{sre} - x^{r0}) * (\partial^2 (LGR_3(x))/\partial x^2)(x_{sre} - x^{r0})\} / \{LGR_3(x_{sre}) * (\partial^2 (LGR_3(x))/\partial x^2)(x_{sre})\} = E_{IN}(x_{sre} - x_0) / E_{IN}(x_{sre}) \quad (9)$$

$\rho^{(4)} = (-\sigma \pm \sqrt{\sigma^2 - \tau}) / 2$
$\rho^{(3)} = [(\theta_{10} - \lambda * \mu) / \theta_6] / \rho^{(4)}$
$\rho^{(2)} = \{-\varphi \pm [\varphi^2 - (\tau / \rho^{(4)} \rho^{(3)})]^{1/2}\} / 2$
$\rho^{(1)} = [-(\theta_7 / \theta_6) - \rho^{(4)} - \rho^{(3)} - \rho^{(2)}]$
$\sigma = [(\theta_9 / \theta_6) - [\theta_7 (\theta_{10} - \lambda * \mu) / \theta_6^2]] / \{1 - [(\theta_{10} - \lambda * \mu) / \theta_6)]\}$
$\tau = [4 (\theta_{10} - \lambda * \mu) / \theta_6]$
$\varphi = [(\theta_7 / \theta_6) + \rho^{(4)} + \rho^{(3)}]$

Table 3. Solution of Eq. (13)

Above equation was already used for linear and B-Splines interpolation functions [8, 9]. It is calculated here as:

$$\lambda = LGR_3(x_{sre}) * (\partial^2 (LGR_3(x))/\partial x^2)(x_{sre}) = \{f(0) + \theta^{(1)} [(1/2) |x_{sre}|^3 - |x_{sre}|^2 - (1/2) |x_{sre}| + 1] + \theta^{(2)} [-(1/6) |x_{sre}|^3 + |x_{sre}|^2 - (11/6) |x_{sre}| + 1]\} * \{\theta^{(1)} (3 |x_{sre}| - 2) + \theta^{(2)} (-|x_{sre}| + 2)\} \quad (10)$$

$$\mu = E_{IN}(x_{sre} - x_0) / E_{IN}(x_{sre}) = [(x_{sre} - x_0)^5 \theta_5 + (x_{sre} - x_0)^4 \theta_4 + (x_{sre} - x_0)^3 \theta_3 + (x_{sre} - x_0)^2 \theta_2 + (x_{sre} - x_0) \theta_1] / [x_{sre}^5 \theta_5 + x_{sre}^4 \theta_4 + x_{sre}^3 \theta_3 + x_{sre}^2 \theta_2 + x_{sre} \theta_1] \quad (11)$$

The solution of Eq. (9) therefore leads to the following novel re-sampling locations:

$$x^{r(k,i)} = (x_{sre}^{(i)} - \rho^{(k)} x_{sre}^{(i)}),\ i = 1,2…4;\ k = 1,2…4 \quad (12)$$

where:

$$\rho^4 \theta_6 + \rho^3 \theta_7 + \rho^2 \theta_8 + \rho \theta_9 + (\theta_{10} - \lambda * \mu) = 0 \quad (13)$$

has its solution is reported in Table 3, while the theta values are reported in Table 1.

2.6 Characterization of the Interpolation Error Improvement and Interpolation Error Bounds

2.6.1. Definition I

Let $\mathbf{f}$: $R^n \rightarrow R^n$ the n^{-th} dimensional function to approximate, and let $\mathbf{x}$: $R^n \rightarrow R^n$ its domain. In real applications, $\mathbf{f}$ is constituted by the discontinuous (discrete) set of values by which the signal is represented. Let be $\mathbf{f(0)}$ the value at the node. Let the n^{-th} dimensional interpolation function $\mathbf{h}$: $R^n \rightarrow R^n$ be represented by $\mathbf{h(x)} = \Sigma_k \alpha_k \beta_k(\mathbf{x})$, of which Eq. (2) furnishes an example in one dimension, and let $\mathbf{x}$: $R^n \rightarrow R^n$ its domain of existence. Let us assume $\mathbf{h}$ and $\mathbf{f}$ be continuous and such that it exist their non-null derivatives up to the second order.

In the remainder of the text the notation: $(\partial^2 (\mathbf{h(x)}) / \partial x_p \partial x_q) (\mathbf{x_{sre}}^{(i)})$ is the second order derivative of $\mathbf{h(x)}$, with respect to the variables x_p and x_q, calculated at the location $(\mathbf{x_{sre}}^{(i)})$. Also, $(\partial^2 (\mathbf{h(x)}) / \partial x_p \partial x_q) (\mathbf{x_{sre}}^{(i)} - \mathbf{x}^{r(k,\,i)})$ is the second order derivative of $\mathbf{h(x)}$, with respect to the variables x_p and x_q, calculated at the location $(\mathbf{x_{sre}}^{(i)} - \mathbf{x}^{r(k,\,i)})$.

2.6.2. Lemma I

By means of the theory there exists: (i) for $\mathbf{h}$ a spatial set of points called the Sub-pixel Efficacy Region $\mathbf{x_{sre}}^{(i)} \in \{\mathbf{x} : \partial (\Delta E(\mathbf{x})) / \partial x_p = 0,\ p = 1,2\ldots n\}$, $i = 1, 2\ldots s$, where s is the degree of the polynomial $\partial (\Delta E(\mathbf{x})) / \partial x_p = 0$, $p = 1, 2\ldots n$; and (ii) for the sampling location $\mathbf{x} = \mathbf{x_0}$, a novel re-sampling location $\mathbf{x}^{r0} \in \{\mathbf{x}^{r(k,\,i)},\ k = 1, 2\ldots t;\ i = 1, 2\ldots s\}$, where t is degree of the polynomial in $\mathbf{x}^{r(k,\,i)}$ as given by:

$$\mathbf{h}(\mathbf{x_{sre}}^{(i)} - \mathbf{x}^{r(k,\,i)}) = \{ E_{IN}(\mathbf{x_{sre}}^{(i)} - \mathbf{x}^{r(k,\,i)}) / E_{IN}(\mathbf{x_{sre}}^{(i)}) \} * \mathbf{h}(\mathbf{x_{sre}}^{(i)}) * \{ \Sigma_{pq} (\partial^2 (\mathbf{h(x)}) / \partial x_p \partial x_q) (\mathbf{x_{sre}}^{(i)}) / \Sigma_{pq} (\partial^2 (\mathbf{h(x)}) / \partial x_p \partial x_q) (\mathbf{x_{sre}}^{(i)} - \mathbf{x}^{r(k,\,i)}) \}\ p \neq q,\ p > q,\ q = 1, 2\ldots n \quad (14)$$

For $\mathbf{x_0}$ and $\mathbf{x}^{r0}$ it is true that: $\| \mathbf{x_0} - \mathbf{x}^{r0} \|_L^2 \leq \boldsymbol{\ell}$, $\| \mathbf{x_0} - \mathbf{x_{sre}}^{(i)} \|_L^2 \leq \boldsymbol{\ell}$, and $\| \mathbf{x}^{r0} - \mathbf{x_{sre}}^{(i)} \|_L^2 \leq \boldsymbol{\ell}$, $i = 1, 2\ldots s$; where $\boldsymbol{\ell}$ is the resolution (sampling step). Let $\mathbf{x_m} = \max \{\| \mathbf{x_0} \|_L^2, \| \mathbf{x_{sre}}^{(i)} \|_L^2, \| \mathbf{x}^{r0} \|_L^2, i = 1, 2\ldots s\}$. Eq. (12) furnishes an example of $\mathbf{x}^{r0}$ in one dimension.

Let $I_E(\mathbf{x_0}) = \| \mathbf{h(x_0)} - \mathbf{h}(\mathbf{x}^{r0}) \|_L^2$ be the interpolation error improvement at $\mathbf{x}_0$, and $C^{(1)}$ and $C^{(2)}$ two constants for which it is true that $C^{(1)} \leq \| \mathbf{h}(\mathbf{x_0}) - \mathbf{h}(\mathbf{x}^{r0}) \|_L^2 \leq C^{(2)}$. Finally let $I_\varepsilon(\mathbf{x_0}) = \| \mathbf{f}(\mathbf{x_0}) - \mathbf{h}(\mathbf{x}^{r0}) \|_L^2$ be the interpolation error at $\mathbf{x}_0$, and $C^{(3)}$ and $C^{(4)}$ two constants for which it is true that $C^{(3)} \leq \| \mathbf{f}(\mathbf{x_0}) - \mathbf{h}(\mathbf{x}^{r0}) \|_L^2 \leq C^{(4)}$.

2.6.3. Lemma II

The general expression that can be derived from Eq. (12) is:

$$\mathbf{h}(\mathbf{x}^{r(k,\,i)}) = F(\mathbf{x_{sre}}^{(i)}, \mathbf{x}^{r(k,\,i)}) \quad (15)$$

where F expresses the dependency of $\mathbf{h}$ on $\mathbf{x_{sre}}^{(i)}$ and $\mathbf{x}^{r(k,\,i)}$. Let the sampling location be $\mathbf{x}_0$, and let the novel re-sampling locations computed from Eq. (12) be $\mathbf{x}^{r(k,\,i)}$, $k = 1, 2\ldots t$; $i = 1, 2\ldots s$. Let $\mathbf{x_{sre}}^{(m)} \in \{\mathbf{x_{sre}}^{(i)}, i = 1, 2\ldots s\}$ and $\mathbf{x}^{r(b,\,m)} \in \{\mathbf{x}^{r(k,\,i)}, k = 1, 2\ldots t;\ i = 1, 2\ldots s\}$ such that: $F_{max} = F(\mathbf{x_{sre}}^{(m)}, \mathbf{x}^{r(b,\,m)}) \geq F(\mathbf{x_{sre}}^{(i)}, \mathbf{x}^{r(k,\,i)})$ for $k = 1, 2\ldots t$; $i = 1, 2\ldots s$. Let $\mathbf{x_{sre}}^{(e)} \in \{\mathbf{x_{sre}}^{(i)}, i = 1, 2\ldots s\}$ and $\mathbf{x}^{r(b,\,e)} \in \{\mathbf{x}^{r(k,\,i)}, k = 1, 2\ldots t;\ i = 1, 2\ldots s\}$ such that: $F_{min} = F(\mathbf{x_{sre}}^{(e)}, \mathbf{x}^{r(b,\,e)}) \leq F(\mathbf{x_{sre}}^{(i)}, \mathbf{x}^{r(k,\,i)})$ for $k = 1, 2\ldots t$; $i = 1, 2\ldots s$. It is true that:

$$\lim_{\mathbf{x_0} \rightarrow \mathbf{0}} \| \mathbf{h}(\mathbf{x_0}) - \mathbf{h}(\mathbf{x}^{r(k,\,i)}) \|_L^2 \geq \lim_{\mathbf{x_0} \rightarrow \mathbf{0}} \| \mathbf{h}(\mathbf{x_0}) - F_{max} \|_L^2 = \| \mathbf{f(0)} - F_{max} \|_L^2 = C_1 \quad (16.a)$$

$$\lim_{\mathbf{x_0} \rightarrow \mathbf{0}} \| \mathbf{f}(\mathbf{x_0}) - \mathbf{h}(\mathbf{x}^{r(k,\,i)}) \|_L^2 \geq \lim_{\mathbf{x_0} \rightarrow \mathbf{0}} \| \mathbf{f}(\mathbf{x_0}) - F_{max} \|_L^2 = \| \mathbf{f(0)} - F_{max} \|_L^2 = C_1 \quad (16.b)$$

$$\lim_{\mathbf{x_0} \rightarrow \mathbf{x_m}} \| \mathbf{h}(\mathbf{x_0}) - \mathbf{h}(\mathbf{x}^{r(k,\,i)}) \|_L^2 \geq \lim_{\mathbf{x_0} \rightarrow \mathbf{x_m}} \| \mathbf{h}(\mathbf{x_0}) - F_{max} \|_L^2 = \| \mathbf{h}(\mathbf{x_m}) - F_{max} \|_L^2 = C_3 \quad (16.c)$$

$$\lim_{\mathbf{x_0} \rightarrow \mathbf{x_m}} \| \mathbf{f}(\mathbf{x_0}) - \mathbf{h}(\mathbf{x}^{r(k,\,i)}) \|_L^2 \geq \lim_{\mathbf{x_0} \rightarrow \mathbf{x_m}} \| \mathbf{f}(\mathbf{x_0}) - F_{max} \|_L^2 = \| \mathbf{f}(\mathbf{x_m}) - F_{max} \|_L^2 = C_{3\text{-}f} \quad (16.d)$$

$$\lim_{\mathbf{x_0} \rightarrow \mathbf{0}} \| \mathbf{h}(\mathbf{x_0}) - \mathbf{h}(\mathbf{x}^{r(k,\,i)}) \|_L^2 \leq \lim_{\mathbf{x_0} \rightarrow \mathbf{0}} \| \mathbf{h}(\mathbf{x_0}) - F_{min} \|_L^2 = \| \mathbf{f(0)} - F_{min} \|_L^2 = C_2 \quad (16.e)$$

$$\lim_{\mathbf{x_0} \rightarrow \mathbf{0}} \| \mathbf{f}(\mathbf{x_0}) - \mathbf{h}(\mathbf{x}^{r(k,\,i)}) \|_L^2 \leq \lim_{\mathbf{x_0} \rightarrow \mathbf{0}} \| \mathbf{f}(\mathbf{x_0}) - F_{min} \|_L^2 = \| \mathbf{f(0)} - F_{min} \|_L^2 = C_2 \quad (16.f)$$

$$\lim_{\mathbf{x_0} \rightarrow \mathbf{x_m}} \| \mathbf{h}(\mathbf{x_0}) - \mathbf{h}(\mathbf{x}^{r(k,\,i)}) \|_L^2 \leq \lim_{\mathbf{x_0} \rightarrow \mathbf{x_m}} \| \mathbf{h}(\mathbf{x_0}) - F_{min} \|_L^2 = \| \mathbf{h}(\mathbf{x_m}) - F_{min} \|_L^2 = C_4 \quad (16.g)$$

$$\lim_{\mathbf{x_0} \rightarrow \mathbf{x_m}} \| \mathbf{f}(\mathbf{x_0}) - \mathbf{h}(\mathbf{x}^{r(k,\,i)}) \|_L^2 \leq \lim_{\mathbf{x_0} \rightarrow \mathbf{x_m}} \| \mathbf{f}(\mathbf{x_0}) - F_{min} \|_L^2 = \| \mathbf{f}(\mathbf{x_m}) - F_{min} \|_L^2 = C_{4\text{-}f} \quad (16.h)$$

Where for $\mathbf{x_0} \rightarrow \mathbf{0}$, $\mathbf{h(x_0)} = \mathbf{f(0)}$, and it is assumed $\mathbf{f(x_0)} = f(\mathbf{0})$. C_1, C_2, C_3, C_4, $C_{3\text{-}f}$, and $C_{4\text{-}f}$ are constants. Let $C^{(1)} = \min \{C_1, C_2, C_3, C_4\}$, $C^{(2)} = \max \{C_1, C_2, C_3, C_4\}$, $C^{(3)} = \min \{C_1, C_{3\text{-}f}, C_2, C_{4\text{-}f}\}$, and $C^{(4)} = \max \{C_1, C_{3\text{-}f}, C_2, C_{4\text{-}f}\}$. Therefore, it follows that:

$$C^{(1)} \leq \| \mathbf{h}(\mathbf{x_0}) - \mathbf{h}(\mathbf{x}^{r0}) \|_L^2 \leq C^{(2)} \quad (17)$$

$$C^{(3)} \leq \| \mathbf{f}(\mathbf{x_0}) - \mathbf{h}(\mathbf{x}^{r0}) \|_L^2 \leq C^{(4)} \quad (18)$$

Theorem I

Eq. (15) is Condition Necessary and Sufficient (CNS) for being: $C^{(1)} \leq \| \mathbf{h}(\mathbf{x_0}) - \mathbf{h}(\mathbf{x}^{r0}) \|_L^2 \leq C^{(2)}$.

Proof

If Eq. (15) is true, from Lemma II it follows that Eq. (17) is verified. If Eq. (15) is false, that is $\mathbf{h}(\mathbf{x}^{r(k,\,i)}) \neq F(\mathbf{x_{sre}}^{(i)}, \mathbf{x}^{r(k,\,i)})$, then it must be false that $C^{(1)} \leq \| \mathbf{h}(\mathbf{x_0}) - \mathbf{h}(\mathbf{x}^{r0}) \|_L^2 \leq C^{(2)}$. Thus Eq. (15) is necessary for Eq. (17) to be true. If Eq. (17) is true, then it must be true that Eq.

(15) is verified. Therefore Eq. (15) is CNS to Eq. (17), which proofs the theorem.

An immediate implication of the theorem is that for any given intra-pixel locations $\mathbf{x}_0$, $\mathbf{x}^{r0} \in [\mathbf{0}, \mathbf{x}_m]$, the interpolation error improvement at $\mathbf{x}_0$:

$$I_E(\mathbf{x}_0) = \| \mathbf{h}(\mathbf{x}_0) - \mathbf{h}(\mathbf{x}^{r0}) \|_L^2 \quad (19)$$

is bounded by two constants: $C^{(1)}$ and $C^{(2)}$.

Theorem II

Eq. (15) is Condition Necessary and Sufficient (CNS) for being: $C^{(3)} \leq \| \mathbf{f}(\mathbf{x}_0) - \mathbf{h}(\mathbf{x}^{r0}) \|_L^2 \leq C^{(4)}$.

Proof

If Eq. (15) is true, from Lemma II it follows that Eq. (18) is verified. If Eq. (15) is false, that is $\mathbf{h}(\mathbf{x}^{r(k,\,i)}) \neq F(\mathbf{x}_{sre}^{(i)}, \mathbf{x}^{r(k,\,i)})$, then it must be false that $C^{(3)} \leq \| \mathbf{f}(\mathbf{x}_0) - \mathbf{h}(\mathbf{x}^{r0}) \|_L^2 \leq C^{(4)}$. Thus Eq. (15) is necessary for Eq. (18) to be true. If Eq. (18) is true, then it must be true that Eq. (15) is verified. Therefore Eq. (15) is CNS to Eq. (18), which proofs the theorem.

Therefore for any given intra-pixel location $\mathbf{x}_0$, $\mathbf{x}^{r0} \in [\mathbf{0}, \mathbf{x}_m]$, the interpolation error at $\mathbf{x}_0$:

$$I_\varepsilon(\mathbf{x}_0) = \| \mathbf{f}(\mathbf{x}_0) - \mathbf{h}(\mathbf{x}^{r0}) \|_L^2 \quad (20)$$

is bounded by two constants: $C^{(3)}$ and $C^{(4)}$.

While $C^{(1)}$ and $C^{(2)}$ depend on the value given by the interpolation function, $C^{(3)}$ and $C^{(4)}$ depend on the value given by the function to approximate, the four of them, consequentially to the formulation of $\mathbf{x}_{sre}^{(i)}$ and $\mathbf{x}^{r(k,\,i)}$ depend also on values expressing relationships between the intra-pixel location $\mathbf{x}_0$ and pixel intensity at the neighbourhood.

3. Results

3.1 Validation Methodology

To demonstrate the improved approximation properties of the Lagrange interpolation, two validation approaches were undertaken. These are: the study of the Fast Fourier Transform (FFT) spectral analysis and the study the root-mean-square-error (RMSE). In order to show the improved approximation offered by the Sub-pixel Efficacy Region for both of the two types of validation approaches, two-dimensional images were shifted along one dimension at intra-pixel locations x_0. They were motion corrected and interpolated at the location x_0, and also at the novel re-sampling location x^{r0} as per Eq. (12). At the aim to simplify, in the remainder of the text, to indicate that the signal or the image was motion corrected and interpolated, the term processed will be used. While processing the image using x_0 will be referred as the classic Lagrange interpolation, processing using x^{r0} will be referred as the SRE-based Lagrange interpolation. The FFT spectral analysis consisted of the evaluation of the deviations from the spectrum of the original image, of those spectra obtained using classic Lagrange and SRE-based Lagrange interpolation functions. For the RMSE analysis, the metric $R = (1 - RMSE^{before} / RMSE^{after})$ was evaluated, where $RMSE^{before}$ was calculated using classic Lagrange interpolation, and $RMSE^{after}$ was calculated using SRE-based Lagrange interpolation. Values of misplacement are reported throughout the text and in the figures as pure numbers with the intent that the behaviour of the RMSE for varying misplacement is seen as a lookup table for corresponding values of sampling resolution.

3.2 Image Data

The data used in this research consisted of the following: (i) A Magnetic Resonance Image (MRI) volume (18 slices) and a functional MRI volume (16 slices) of the human brain. These had respectively axial resolution of 128 x 128 [2.0 x 2.0 mm], and 64 x 64 [3.75 x 3.75 mm], and 6.00 mm inter-slice resolution; (ii) A 238 x 253 MRI sagittal slice; (iii) 208 x 222 "Lena" image used as original for the FFT analysis, and sub-sampled to 128 x 128 for the RMSE analysis; (iv) Three cell images and one microscopic cell image (Diatoms) having respectively 512 x 512 and 128 x 128 as matrix resolution. To avoid aliasing, the original matrix resolution of 256 x 256 was employed for the FFT analysis of the MRI volume. For MRI and functional MRI volumes, the metric R was computed as the sum of 18 and 16 values respectively, with each being calculated for a slice of the volume.

3.3 FFT spectral Analysis

The FFT spectral analysis aims to show that it exist differences between the spectrum of the original image, the spectrum of the image processed with classic Lagrange interpolation, and the spectrum of the image processed with SRE-based Lagrange interpolation. Therefore, the spectral energy of the original image (O_E) was compared to the spectral energy of the image processed with the classic Lagrange function (NOSRE_E), and the spectral energy of the image processed with the SRE-based Lagrange function (SRE_E). FFTs were shifted so to have zero frequency signals at the centre of the spectrum. The spectral analyzer was built on 2000 of equally spaced FFT magnitudes intervals and the analysis was focused on the highest energy range, and thus intervals from 970 through 1036 were analyzed. The value abs(O_E - SRE_E) - abs(O_E - NOSRE_E) was calculated at each interval for a misplacement $x_0 = 0.87$ in all cases. Figure 1 shows an MRI volume's slice (a); a functional MRI slice (b); and "Lena" (c), with their respective frequency spectra analyzers in (d), (e) and (f). Values below zero indicate that the SRE-based Lagrange interpolation function determines the resulting image as such to incorporate frequencies that more closely match the original image's spectrum. Positive values indicates the opposite, that is, the classic Lagrange interpolation function produces frequencies that do match with those of the original image more closely than the SRE-based Lagrange interpolation function does. Figure 2 shows results for the sagittal MRI: frequency spectra analyzer (a); pixels corresponding to the frequency components shown in black in figure 2a as white overlay onto the original image (b); subtraction between the root-square

image (RSE) obtained with classic Lagrange interpolation and the RSE obtained with SRE-based Lagrange interpolation (c).

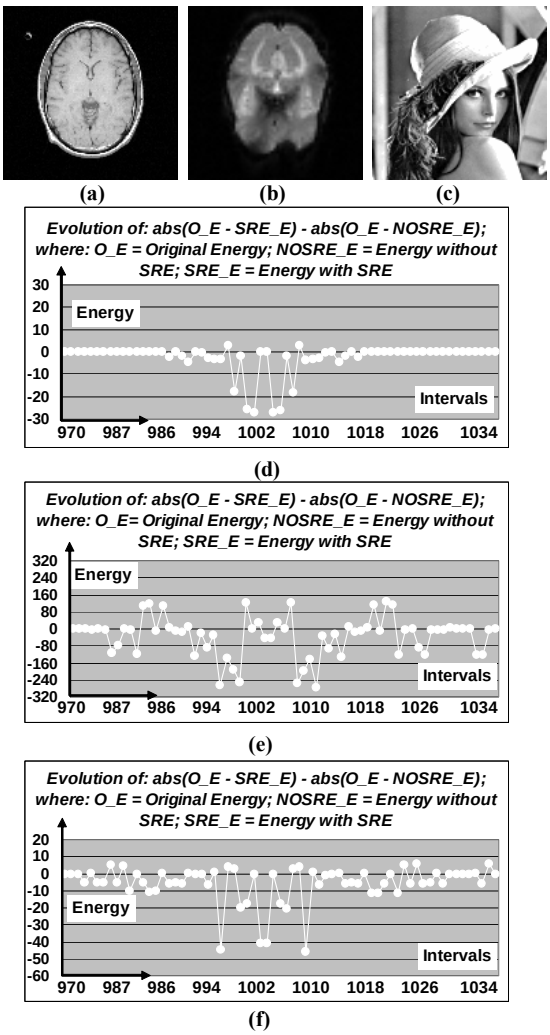

Figure 1. FFT spectral analysis. Original images: MRI (a), functional MRI (b), and "Lena" (c), and their respective frequency spectra evolutions after motion correction and interpolation: (d), (e) and (f). While values below zero indicates that the SRE-based Lagrange function was superior to the classic, values above zero indicates the opposite.

3.4 RMSE Analysis

Data were shifted at steps of 0.001, along one dimension (x), of misplacements within the range [0, 0.109] and then processed with classic and SRE-based Lagrange interpolation functions. Figure 3 shows (a) the behavior of R with varying misplacements for: the functional MRI volume (curve 1), the MRI volume (curve 2), the sagittal MRI slice (curve 3), and for "Lena" in (b). While white indicates improvement of the SRE-based Lagrange interpolation function over the classic, black indicates the opposite. For the three cell images, respectively in (a), (b) and (c) of figure 4, it is shown the resulting improvement by the respective plots of R versus misplacement: (d), (e) and (f). Another set of experiments show the results obtained on the same set of data (Diatoms' image) by the use of the Sub-pixel Efficacy Region on three more interpolation paradigms: bivariate linear, quadratic and cubic B-Splines.

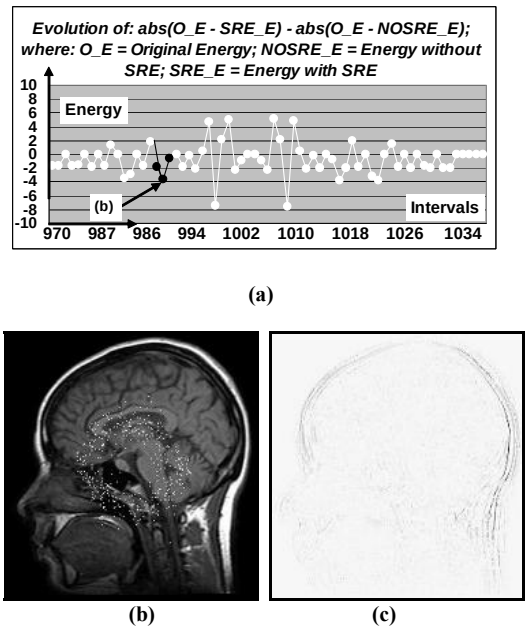

Figure 2. FFT spectral analysis. In (a) spectra evolution for the sagittal slice after motion correction and interpolation. In (b) pixels (white) corresponding to the particular spectral energy values indicated in black in (a). RSE image resulting after the subtraction between images obtained by classic and the SRE-based interpolation functions (c).

Figures 5a and 5b show two images obtained after they were processed with a misplacement of $x_0 = 0.006$ by the classic quadratic B-Spline and the SRE-based bivariate linear interpolation. The latter shows that for small misplacements performances are comparable to the former. In the rest of figure 5, each graph shows R consisting of the improvement obtained with the SRE-based interpolation paradigm over the classic paradigm, respectively for bivariate linear (c), quadratic B-Spline (d), and cubic B-Spline (e). While the equations of classic bivariate linear and quadratic B-Spline are given in the appendix, the mathematical formulations of their SRE-based paradigms are given in [8, 9]. Figure 6 shows, for some data set, curves that indicate the percentage improvement of the SRE-based Lagrange function (LGR-SRE) over SRE-based quadratic ($h_3(x)$) and cubic ($h_4(x)$) B-Spline functions (SPLINE-SRE). All curves are in logarithmic scale and they report the value $I = \ln [(R^{LGR-SRE} / R^{SPLINE-SRE}) * 100]$. The first and the second curve from the top are relevant respectively to the sagittal MRI and the fMRI volume for the improvement over the cubic SRE-based B-Spline. The third curve from the top is relevant to the MRI volume for the improvement over the quadratic SRE-based B-Spline. The fourth curve is relevant to the sagittal MRI and, coincidentally, also to the fMRI volume, and indicates improvement over the quadratic SRE-based B-Spline. In general, based on the present comparison, the Lagrange improvement was between $\exp^{12} / 100$ and $\exp^{3} / 100$ of the B-Spline improvement.

3.5 Lagrange Bounds for the Interpolation Error and the Interpolation Error Improvement

To ascertain the magnitude of dependency on the resolution of interpolation error improvement and the interpolation error, given that no assumption was made

on the nature of the relationship between interpolation error and sampling step, it is natural to refer to the data

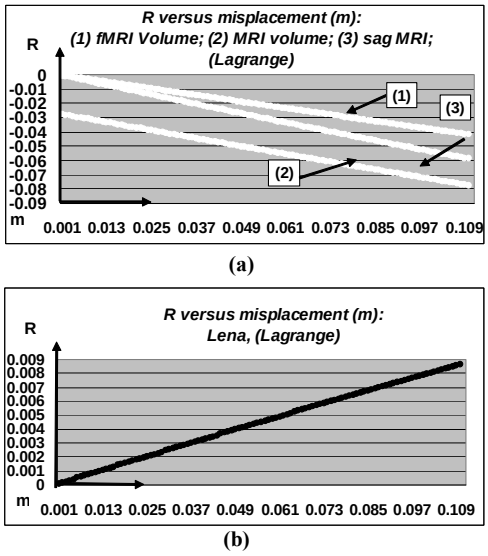

Figure 3. Ratio of improvement resulting from the RMSE analysis. In (a) functional MRI, MRI, and sagittal MRI; "Lena" in (b). While white indicates superiority of SRE-based Lagrange interpolation, black indicates superiority of the classic paradigm.

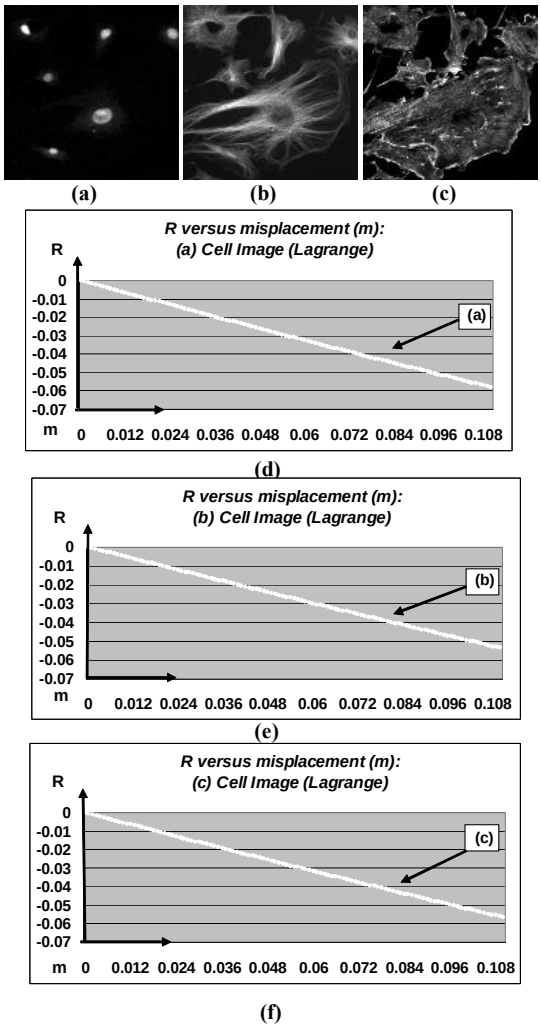

Figure 4. Cell's images (a), (b) and (c), and result of the RMSE analysis: (d), (e), (f).

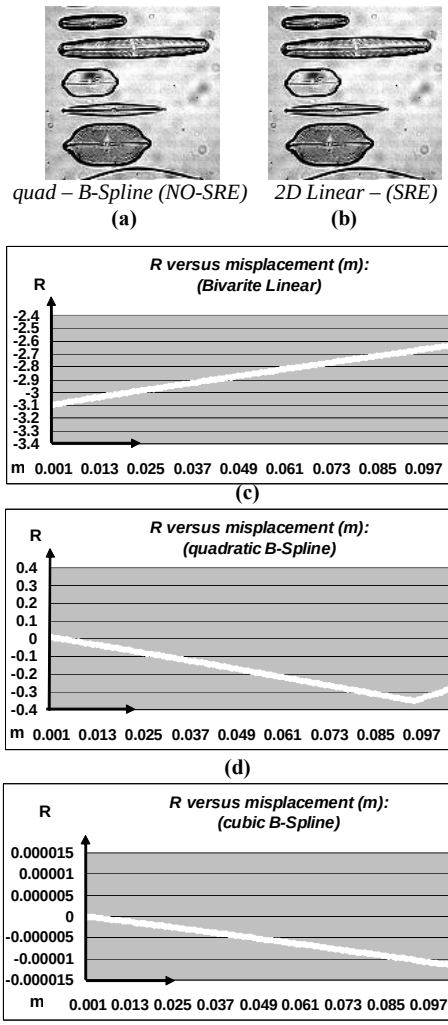

Figure 5. Comparison across SRE-based interpolation paradigms based on the Diatom's image. In (a) image obtained by classic quadratic B-Spline to compare to that in (b) obtained by SRE-based bivariate linear. Plots of *R*: (c) SRE-based bivariate, (d) quadratic, and (e) cubic SRE-based B-Splines.

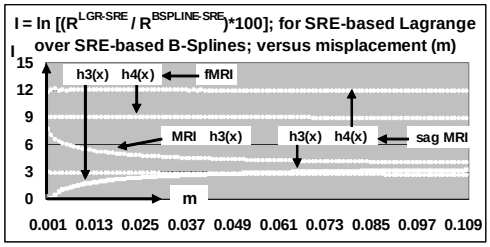

Figure 6. *R* values comparison between SRE-based Lagrange (LGR-SRE) and SRE-based B-Splines (SPLINE-SRE). Logarithmic plot versus misplacement of $I = \ln [(R^{LGR\text{-}SRE} / R^{SPLINE\text{-}SRE}) * 100]$ for: sagittal MRI, functional MRI and MRI volumes.

obtained by the estimation of signals at unknown locations such to clarify for varying resolution, the behaviour of variation of the interpolation error and its improvement based on SRE. This presentation is anticipated from what has been previously seen by the data presented in [8, 9], that is: while estimating the signals at unknown locations, results show that the interpolation error improvement is determined regardless of varying resolution being itself achieved for different

intra-nodal distances. It is thus natural to ask the question as to how the change of interpolation error and its improvement behaves for varying resolution, and also what is the magnitude of the bounds that were demonstrated by Theorems I and II.

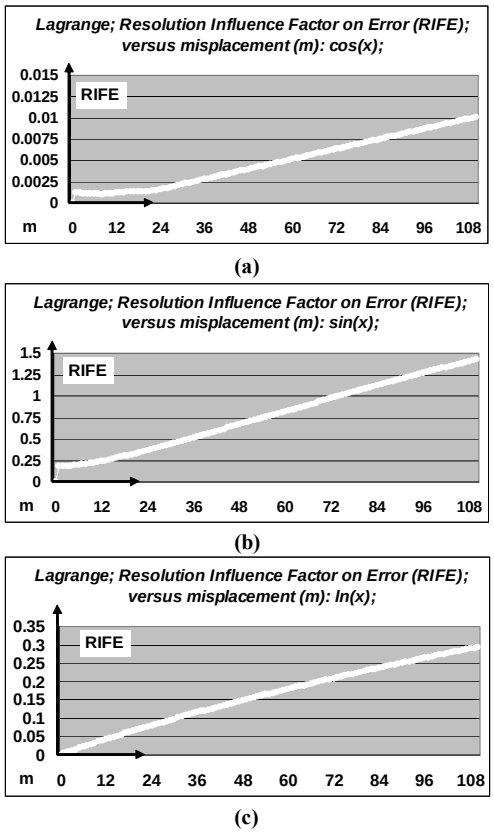

Figure 7. Influence of the Resolution on the Interpolation Error: Lagrange. The influence factor (RIFE) is displayed versus the misplacement for cos (x) in (a), sin (x) in (b), and ln (x) in (c). The actual misplacement is given by m*0.01 for 0.1 resolution, and by m*0.0001, for of 0.01 and 0.001 resolutions. For each of the misplacements, the pictures display the overall RIFE obtained computing based on the three sampling resolutions of 0.1, 0.01, and 0.001.

For cos (x), sin (x) and for ln (x), the behaviour of the influence of the resolution on the interpolation error for the Lagrange function will be indicated by the Resolution Influence Factor on Error (RIFE). Also, the influence of the resolution on the interpolation error improvement will be indicated by the Resolution Influence Factor on Improvement (RIFI). These factors were calculated summing up the following three values of absolute difference, each of which computed between the interpolation errors obtained by the SRE-based function, while estimating the signal for 111 samples at two given resolutions: (i) 0.1 and 0.01; (ii) 0.1 and 0.001; (iii) 0.01 and 0.001. The sum of these three values should be ideally zero if there wasn't any effect of the resolution on the interpolation error as well on the improvement of the interpolation error obtained by the SRE-based function versus the corresponding classic. Figures 7 and 8 shows RIFE and RIFI factors when the SRE-based Lagrange function is employed in the estimation of the three signals respectively. Overall the RIFE factor was below $1.5 / (3 * 111) = 4.5 * 10^{-3}$. The RIFI factor was below $400 / (3 * 111) = 1.2$. Thus, relatively to the experimentation conducted here, the lower bounds were 0, and the upper bounds were $4.5 * 10^{-3}$ and 1.2 for the Interpolation Error and the Interpolation Error Improvement respectively.

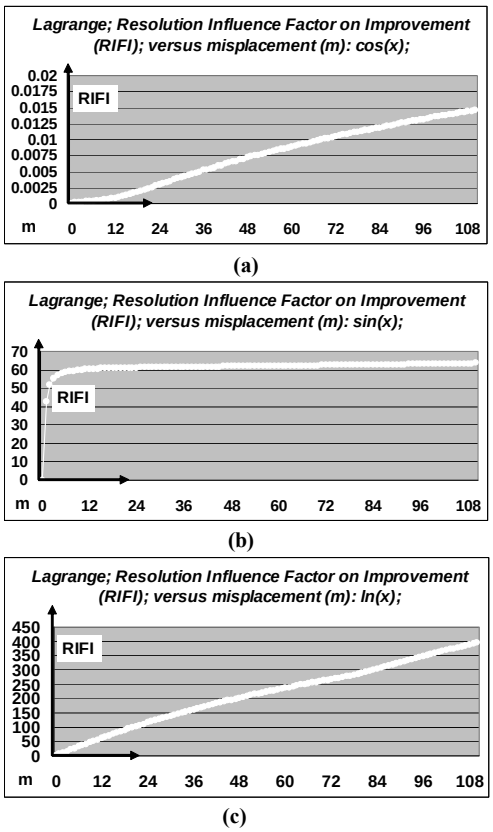

Figure 8. Influence of the Resolution on the Improvement of the Interpolation Error: Lagrange. The influence factor (RIFI) is displayed versus the misplacement for cos (x) in (a), sin (x) in (b), and ln (x) in (c). The misplacement is displayed as per figure 7 for same sampling resolution.

4. Discussion and Conclusions

4.1 Literature

For image processing applications such as signal reconstruction or signal interpolation, Lagrange polynomials were derived such that their coefficients depend on the sum of digital signals [11], or on linear combination of the data to interpolate [2, 10], or on the sampling step [12, 13]. Similarities between Lagrange and Sinc interpolation functions were demonstrated in first instance [14], and later it was pointed out [10] that for a given termination of the series' order terms, the former constitutes an approximate expression of the latter. That is, the Lagrange function approximates the Sinc, as much as higher order terms of its series are incorporated into the polynomial. Also, multiplying the Lagrange function by the Sinc function, the latter being windowed by the binomial distribution, it became possible to obtain a Lagrange polynomial with improved stop-band characteristics [15]. The present work dedicates efforts in deriving an improved version of the Lagrange interpolation. This is done within the task of extending the unifying framework presented in [8, 9].

Within the context of the study of interpolation error representations [16], error bounds for B-Splines were reported [17, 18] which were derived from results obtained in approximation theory in [4] and that consistently asserted the general proposition of the dependency of the interpolation error on the sampling step h, and precisely of the order $O(h^n)$; where n is the order of the quasi-interpolation function. Concluding from such error representation approach, is the fact that the interpolation error tends to be null for a sampling step $h \rightarrow 0$.

Such form of error bound representation, of which a complete characterization is given in [19], was later recalled in [5-7, 20-22], and based on it: (i) an expression for the Gaussian interpolation function was reported in [23] as based on the work published in [24], (ii) the parameterization of piecewise-polynomial interpolation kernels was given in [25], and (iii) a novel scheme of linear interpolation was later determined [26].

Results published in [4] were also discussed in [17] within the context of B-Spline knot placement, starting from the assertion that for an interpolation function h of the n^{-th} order, the error representation is itself depending on the norm of the n^{-th} order derivative $h^{(n)}$ of the function, and it was also demonstrated in [17] that the minimization of the error bound reported in [4] can be obtained by either determining an optimal knot placement, or determining an optimal step size such that it minimizes the quantity:

$$\max_i \| h(n) \|_{[\zeta i, \zeta i+1]} * | \Delta\zeta i |^n \qquad (21)$$

where $a < \zeta_1 < \ldots < \zeta_m < b$ are the m knots in the interval of definition] a, b [, and $| \Delta\zeta_i |$ is the i^{-th} knot inter-space.

It has been demonstrated in [27] that the existence of error bounds representations for a polynomial interpolator of the form: Pf := f(a) (where $a \in (R^d)$, n is the order of the polynomial, d is the spatial dimensionality) which take the form of: $f(x) - Pf(x) = \Sigma_i R_i (D^{n+1} f)$, where $f \in C^{n+1}(R^d)$, that is: f is continuous up until n+1 order. Also, $\{R_i\}$ represents a collection of functions for which the convolution $R_i \times D^{n+1} f$, is continuous in $C^{n+1}(R^d)$. Expressions of $\{R_i\}$ were derived as dependent on the value of the function $f(a_j)$ at the nodes of the neighborhood K, where $a_j \in K$.

These results extended previous work [28] and were obtained by focusing on the linear interpolation function, and propose for the specific case of bivariate linear function, the existence of a spatial support of the error bound, consisting of a rectangular region which shape in the form: (0, 0), (x, 0), (x, y), and (0, y). Therefore, according to [27, 28], for a polynomial of n^{-th} order, the error bound representation involves the computation of n + 1 derivative and its integration.

As far as the theory proposed for the bivariate linear interpolation function [8], it exhibits consistent similarities with [27, 28]. Particularly, the theory proposed in [8], when examined within the view of the results published in [28], formulates the two Intensity-Curvature terms E_o and E_{IN} as consisting of indirect measures of the interpolation error, and thus it reflects the Intensity-Curvature Functional in the form of the calculation and solution of $\partial (\Delta E(x, y)) / \partial x = 0$; $\partial (\Delta E(x, y)) / \partial y = 0$. Furthermore, the theory determines the extremes of ΔE, and finally it leads to a rectangular region which is called Sub-pixel Efficacy Region (SRE). By means of the SRE, it is possible to determine novel re-sampling location (x^{r0}, y^{r0}). The novel locations improve the interpolation function as far its approximation error is concerned. Within this context, the theory proposed in [8] constitutes, for the particular case of the bivariate linear function, an extension with respect to [27, 28] because it goes beyond the error bound representation and it provides the interpolation function with improved approximation capabilities.

For the Lagrange interpolation function, various error bounds can also be found in literature that are dependent on the sampling step [1] or based on Hilbert transform [3]. Also, the Chebyshev polynomial was used in [2] to identify the optimal nodes to use by the Lagrange function and it determined an error bound form representation which is based on an extension of the work published in [29, 30] that is dependent on the modulus of continuity of the function f to interpolate as per following form:

$$| f(x) - Q_n(f, x) | = O(1)\, \omega(f, \sqrt{1 - x^2}/n) \qquad (22)$$

where $\text{Lim} \| f(x) - Q_n(f, x) \| = 0$, and N is the number of points of f, n is the degree of the polynomial $Q_n(f, x)$, and the modulus of continuity of a function f is defined as $\omega_f (\delta, t) = \max | f(t) - f(s) |$ so that $| s - t | < \delta$. Such an expression of the error bound is implicitly dependent on the degree of the polynomial, but closely resembles those forms based on the sampling step since it is true that the discrepancy between f(x) and $Q_n(f, x)$, as indicated above, tends to zero for an infinite number of points and that is equivalent to the sampling step being almost zero.

4.2 Benefits and Limitations of the SRE

In comparison to the classic interpolation schemes reported in literature, the SRE-based interpolation functions [8, 9] presents two main benefits, which are derived from the application of the conception of the Sub-pixel Efficacy Region.

The first benefit is the determination of frequency components in the re-sampled images that, at least in part, more closely match those of the original image, and this is related to the change in pass-band characteristics due to pixel-by-pixel re-sampling. That re-sampling is done at locations which vary pixel-by-pixel does not constitutes a novelty, however, since Lagrange interpolation has been applied to 2D signal reconstruction based on non-uniform samples [31], and re-sampling of a signal at irregular intervals has been the subject of study [32], being it applied to the Lagrange formula [33]. Sampling at irregular space interval is also related to B-Splines knot optimization strategies, of which, for a review, the reader is referred to [17], and also related to interpolation of scattered data, of which a review is provided in [34].

The second benefit is the reduction of the interpolation error based on the calculation of the Lagrange function at novel re-sampling locations. These are derived from the study of the Intensity-Curvature

Functional which is a mathematical formulation that merges pixel (node) intensity values at the neighbourhood together with the curvature of the interpolation function. This formulation constitutes a novelty with respect to previously reported approaches [5-7].

The theory employed here emerges from novel conceptions and, as such, it is confronted however with undeniable limitations. Thus, it is important to recognize, as the experimental evidence confirms, that the unifying framework assumes in some cases limiting characteristics by (i) not allowing improvement of the interpolation error and (ii) incorporating into the resulting re-sampled signals frequency components that partially mismatch those of the original signal.

4.3 The Contribution made by the SRE-based Interpolation Functions

The improved approximation properties of the Lagrange interpolation function can be potentially generalized to any interpolation function, regardless of dimensionality and degree, provided that the function is continuous in its domain of existence and that there exists second order derivatives [8, 9]. Thus, the task of improving the performance of the Lagrange interpolation function has been accomplished by a novel approach and within the context of a unifying framework. The Intensity-Curvature Functional (ΔE) has been devised as a mathematical methodology capable of embedding in the same formulation both pixel intensity at the neighbourhood and curvature of the interpolation function. By solving the polynomial resulting from the first order derivatives of ΔE, an intra-pixel set of spatial points called the Sub-pixel Efficacy Region (SRE) has been derived, and allowed calculation of the Lagrange function at variable intra-pixel location, with improved approximation characteristics.

Based on the mathematical formulation presented here, two constants set the boundary of both interpolation error and interpolation error improvement. While for the former, the constants depend on the value of the function to approximate, for the latter they depend on the value of the model interpolation function. For either of the two errors, the constants depend also on values expressing relationships between the intra-pixel location where to re-sample and the pixel intensity at the neighbourhood.

Set results from the application of the theory to three more interpolators have been presented to give an overview of a novel class of interpolators: the SRE-based interpolation functions. In this regard, it is of relevance to emphasize that the bridging concept between classic interpolation and SRE-based interpolation is the curvature of the interpolation function.

Finally, it is given the explanation as to why, through the SRE, improved approximation is achieved at the novel re-sampling location. An interpolation scheme h(x) if asked to estimate a signal at a given location x_0, it will be calculated at x^{r0} by the SRE-based interpolation scheme $h(x^{r0})$, such to obtain a more accurate estimate of the unknown signal that needs to be determined at the location x_0. This is illustrated in figure 9 where the true value is represented by the signal to estimate f(x) (red), the SRE-based interpolation furnishes the values $h(x^{r0})$ (blue), and the classic interpolation estimation furnishes the values h(x) (white). Thus, while considering the neighbourhood: f(-2), f(-1), f(0), f(1) and f(2); estimations $h(x_0)$ and $h(x^{r0})$ are obtained at x_0 and x^{r0} and they correspond to the schemes of classic and SRE-based interpolation functions respectively. Since the discrepancy between the value of $h(x_0)$ and $f(x_0)$ is higher than the discrepancy between of $h(x^{r0})$ and $f(x_0)$, re-sampling at the novel location x^{r0} improves the interpolation error.

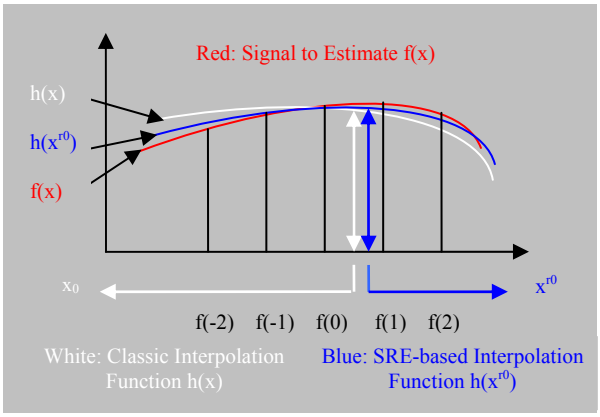

Figure 9: SRE-based versus classic signal interpolation. Blue curve: SRE-based; White curve: classic. Given a location x_0, the discrepancy between the signal to estimate f(x) (red) and the SRE-based estimation at x^{r0} is less than the discrepancy between f(x) and the classic estimation at x_0. Thus, the approximation is improved by re-sampling at x^{r0} in place of x_0.

5. Acknowledgments

Data presented in [8, 9] and in the present paper were obtained through the implementation of the mathematics into Matlab (MathWorks Co.) programs, which were used to re-sample the images employed to validate the properties of the SRE-based interpolation functions. The significance of the SRE is that it provides classic interpolation functions reported in the literature with improved approximation properties. The software that implements the SRE-based interpolation functions it is freely available to the scientific community upon request to Dr. Carlo Ciulla (cxc2728@NJIT.EDU).

Functional MRI volume images were made available by the fMRI Data Center of the Dartmouth College (Hanover, NH) and they recording parameters are described in [35]. "Lena", the cellular image and the Diatom's image were made available by the software package IMAGEJ (http://rsb.info.nih.gov/ij/).

Appendix

A. Equations Used for the Classic Interpolation Paradigms

Bivariate linear:

$$h(x, y) = f(0,0) + x\,(f(1,0) - f(0,0)) + y\,(f(0,1) - f(0,0)) + xy\,(f(1,1) + f(0,0) - f(0,1) - f(1,0)) \quad (A.1)$$

Where: f(0,0), f(1,0), f(0,1) and f(1,1) are the values of intensity at the four corners of the 2D pixel.

Quadratic B-Spline:

$$h_3(x) = \begin{cases} -2a|x|^2 + 1/2\,(a+1) & 0 \le |x| \le ½ \\ a|x|^2 - (2a+1/2)|x| + 3/4\,(a+1) & 1/2 \leqslant |x| \leqslant 3/2 \end{cases} \quad \text{(A.2)}$$

Cubic B-Spline:

$$h_4(x) = \begin{cases} 1/2\,|x|^3 - |x|^2 + 2/3 & 0 \le |x| \le 1 \\ -1/6\,|x|^3 + |x|^2 - 2|x| + 4/3 & 1 \le |x| \le 2 \end{cases} \quad \text{(A.3)}$$

6. References

[1] R. Radzyner and P.T. Bason. An Error Bound for Lagrange Interpolation of Low-Pass Functions. IEEE Trans. Inf. Theory 18: 669-671, 1972.

[2] T. Xie and X. Zhou. A Modification of Lagrange Interpolation. Acta Math. Hungar., 92 (4): 285-297, 2001.

[3] Kubayi, D.G. and Lubinsky, D.S.. A Hilbert Transform Representation of the Error in Lagrange Interpolation. J. Approx. Theory 129: 94-100, 2004.

[4] G. Strang and G. Fix. A Fourier Analysis of the Finite Element Variational Method. Constructive Aspect of Functional Analysis, Cremonese, Rome, Italy pp. 796-830, 1971.

[5] T. Blu and M. Unser. Quantitative Fourier Analysis of Approximation Techniques: Part I – Interpolators and Projectors. IEEE Trans. Sign. Proc., 47 (10): 2783-2795, 1999.

[6] P. Thevenaz, T. Blu and Unser, M. Interpolation Revisited. IEEE Trans. Med. Imag., 19 (7): 739-758, 2000.

[7] T. Blu, P. Thevenaz and M. Unser. .MOMS: Maximal-Order Interpolation of Minimal Support. IEEE Trans. Imag. Proc., 10 (7): 1069-1080, 2001.

[8] C. Ciulla and F.P. Deek. On the Approximate Nature of the Bivariate Linear Interpolation Function: A Novel Scheme Based on Intensity-Curvature. ICGST - International Journal on Graphics, Vision and Image Processing, 5 (7): 9-19, 2005.

[9] C. Ciulla and F.P. Deek..Novel Schemes of Trivariate Linear and One-Dimensional Quadratic B-Spline Interpolation Functions Based on the Sub-pixel Efficacy. ICGST - International Journal on Graphics, Vision and Image Processing, 5 (8): 43-53, 2005.

[10] T. M. Lehmann, C. Gonner and K. Spitzer. Survey: Interpolation Methods in Medical Image Processing. IEEE Trans. Med. Imag., 18 (11): 1049-1075, 1999.

[11] F. Francesconi, G. Lazzari, V. Liberali, F. Maloberti, and G. Torelli. A Novel Interpolator Architecture for ΣΔ DACs. IEEE Proc. 4th Europ. Conf. on Des. Autom., 249-253, 1993.

[12] J.J. Fuchs and B. Delyon. Min-Max Interpolators and Lagrange Interpolation Formula. ISCAS IEEE Int. Symp., 4: IV-429 - IV 432, 2002.

[13] Z. Ye. Linear Phase Lagrange Interpolation Filter Using Odd number of Basepoints. Proc. IEEE ICASSP VI-237- VI-239, 2003.

[14] E.T. Wittaker. On the Functions which are Represented by the Expansion of the Interpolation Theory. Proc. Roy. Soc. Edinburgh 35: 181-194, 1915.

[15] A.G. Dumpster and N.P. Murphy. Lagrange Interpolator Filters and Binomial Windows. Signal Processing 76: 81-91, 1999.

[16] M. Unser and I. Daubechies. On the Approximation Power of Convolution-Based Least Squares Versus Interpolation. IEEE Trans. Sign. Proc., 45: 1697-1711, 1997.

[17] C. De Boor. A practical Guide to Splines. Applied Mathematical Sciences. Springer-Verlag, New York, 1978.

[18] B. D. Bojanov, H. A. Hakopian and A. A. Sahakian. Spline Functions and Multivariate Interpolations, Kluwer Academic Publisher, Dordrecht, The Netherlands, 1993.

[19] C. de Boor, R. A. Devore, and A. Ron. Approximation from Shift Invariant Subspaces of $\mathbf{L}^2(R^d)$, Trans. Amer. Math. Soc., 341: 787-806, 1994.

[20] E. A. Meijering. A Chronology of Interpolation: From Ancient Astronomy to Modern Signal and Image Processing. Proc. IEEE 90 (3): 319-342, 2002.

[21] X. Deng and T. S. Denney, Jr. On Optimizing Knot Positions for Multi-dimensional B-Spline Models. Proc. IS & T SPIE, 2004.

[22] M. Unser. Splines: A Perfect Fit for Signal and Image Processing, IEEE Sign. Proc. Mag., 16: 22-38, 1999.

[23] H. Wendland, Gaussian Interpolation Revisited. In: Trends in Approximation Theory. K. Kopotun, T. Lyche, and M. Neamtu (Eds.). Vanderbilt University Press, Nashville, pp. 417-426, 2001.

[24] W. R. Madych and S. A. Nelson, Bounds on Multivariate Polynomials and Exponential Error Estimates for Multiquadratic Interpolation. J. Approx. Theory 70: 94-114, 1992.

[25] T. Blu, P. Thevenaz, and M. Unser. Complete Parameterization of Piecewise-polynomial Interpolation Kernels. IEEE Trans. Imag. Proc., 12 (11): 1297-1309, 2003.

[26] T. Blu, P. Thevenaz, and M. Unser. Linear Interpolation Revitalized. IEEE Trans. Imag. Proc., 13 (5): 710-719, 2004.

[27] S. Waldron. Minimally Supported Error Representations and Approximation by the Constants. Numer. Math., 85: 469-484, 2000.

[28] S. Waldron. The Error in Linear Interpolation at the Vertices of a Simplex. SIAM J. Numer. Anal., 35: 1191-1200, 1998.

[29] I. Gopengauz. A Theorem of A. F. Timan on the Approximation of Functions by Polynomials on a Finite Segment. Math Zametki, 163-172, 1967.

[30] P. Vertesi. Convergent Interpolatory Processes for Arbitrary Systems of Nodes. Acta Math. Acad. Sci. Hungar., 33: 223-234, 1979.

[31] F.A. Marvasti. Extension of Lagrange Interpolation to 2-D Nonuniform Samples in Polar Coordinates. IEEE Trans. Circ. Syst., 37 (4): 567-568, 1990.

[32] Pr. B. Lacaze. A note about Stationary Process Random Sampling. Stat. & Prob. Lett., 31: 133-137, 1996.

[33] B. Lacaze. About a Multiperiodic Sampling Scheme. IEEE Sign. Proc.Lett., 6 (12): 307-308, 1999.

[34] I. Amidror. Scattered Data Interpolation Methods for Electronic Imaging Systems: A Survey. J. Electr. Imag., 11 (2): 157-176, 2002.

[35] R.L. Buckner, A.Z. Snyder, A.L. Sanders, M.E. Raichle and J.C. Morris. Functional Brain Imaging of Young Non-Demented and Demented Older Adults. Journal of Cognitive Neuroscience, 12-2, 2000.